Available online at www.sciencedirect.com
ScienceDirect
International Journal of Thermal Sciences 47 (2008) 249–260
International Journal of Thermal Sciences
www.elsevier.com/locate/ijts

Infrared nondestructive measurement of thermal resistance between liner and engine block: design of experiment

P. Laloue [a,1], C. Bissieux [b], J.-F. Henry [b], H. Pron [b,*], J. L'Ecolier [a], F. Nigon [a]

[a] *PSA Peugeot Citroën, Laboratoire Optique et Thermique, 45 rue Jean-Pierre Timbaud, 78 300 Poissy, France*
[b] *Université de Reims, Unité de Thermique et Analyse Physique, EA 3802, Laboratoire de Thermophysique, UFR Sciences, Moulin de la Housse, BP 1039, 51 687 Reims Cedex 2, France*

Received 29 August 2005; received in revised form 27 December 2006; accepted 20 February 2007

Available online 21 May 2007

Abstract

Thermal resistances between liners and engine blocks are nondestructively studied by photothermal infrared thermography. Under controlled sinusoidal light irradiation, the thermal response of the sample is measured by means of an infrared camera. A numerical lock-in procedure yields amplitude and absolute phase maps of the thermal field periodic component. Then, apart from classical qualitative detection of air layers, a quantitative characterization of thermal resistance becomes available. An analytical modeling, associated with an inverse procedure using the Gauss–Newton parameter estimation method, allows to identify the thermal resistance on academic samples representative of the liner-engine block interface. Simply joined cast iron and aluminum plates present thermal resistances about 2×10^{-3} K m^2 W^{-1}. The implementation of a numerical modeling allows to study two-dimensional defects. When the samples are pressed on their periphery, thus straightened, contact resistances ranging from 2×10^{-4} to 7×10^{-4} K m^2 W^{-1} have been measured. Then, the method is applied to liner-engine block interfaces where the thermal resistances fall to about 2×10^{-5} K m^2 W^{-1}, matching the values obtained when a cast iron plate is locally pressed against an aluminum plate.

Keywords: Infrared thermography; Thermal resistance; Metal–metal interface; Periodic heat diffusion; Lock-in detection; Thermal model

1. Introduction

In the production process of the PSA engine blocks, the liners are inserted during the casting. Cast iron liners are placed into a mould, in which liquid aluminum is then injected under pressure. This manufacturing technique could cause interface defects that would impede the engine cooling. Currently, this interface is controlled by a destructive technique: the cylinder is cut along three parallel planes and the air layers are measured with an optical microscope. This technique allows to measure extended air layers or located defects, but without a real quantified knowledge of the interface thermal resistance before cutting. So, the development of a nondestructive technique contributes to improve the experimental knowledge of the thermal transfers between liner and engine block and to define more representative thermal limit conditions in the predictive models.

The current trend for nondestructive testing leads notably to thermal nondestructive evaluation of materials associated with inverse methods [1]. The present work, illustrating this research orientation, aims to characterize the variable thermal resistances between liners and engine blocks, and to quantify the thickness of possible air layers that could impede the engine cooling. Since this problem is essentially of thermal nature, photothermal infrared thermography appears to be particularly relevant here. In addition, this nondestructive technique is not disturbed by surface roughness and allows both excitation and detection to be applied on the same side.

The study of the contact between two joined metals was first approached in transient mode with the brief signal method [2]. Then, the use of a periodic thermal field with thermocouples

* Corresponding author. Tel.: +33/0 3 26 91 34 13.
E-mail addresses: peggy.laloue@mpsa.com (P. Laloue), herve.pron@univ-reims.fr (H. Pron).
[1] Tel.: +33/0 1 30 19 44 97.

1290-0729/$ – see front matter
doi:10.1016/j.ijthermalsci.2007.02.012

Nomenclature

Roman letters

a_i	thermal diffusivity of layer i	$m^2\,s^{-1}$
$A_i, B_i, C_i, D_i, E_i, F_i, G_i, H_i, A_{i,n}, B_{i,n}, E_{i,n}$	integration constants	K
f	modulation frequency	Hz
h_0, h_4	heat transfer coefficient at the front/rear face	$W\,m^{-2}\,K^{-1}$
I_0, P_i, M_i	radiative flux	$W\,m^{-2}$
J_0	Bessel function of the first kind of zero order	
k_i	thermal conductivity of layer i	$W\,m^{-1}\,K^{-1}$
K_i	absorption coefficient of layer i	m^{-1}
l_i	thickness of layer i	m
m_n	eigenvalues for spatial frequency	m^{-1}
q_i	volumic heat source in layer i	$W\,m^{-3}$
r	radial coordinate, in the plane of the sample surface	m
r_0	source beam radius at $1/e$	m
t	time	s
T, T_a, T_c, T_{amb}	temperature	K
z	space coordinate, normal to the surface of the sample	m
R	thermal resistance	$K\,m^2\,W^{-1}$

Greek letters

β	parameter under estimation	
μ_i	thermal diffusion length of layer i	m
Φ_i	radiative flux in layer i	$kg\,m^{-3}$
ω	pulsation	$rd\,s^{-1}$

measurements for thermal resistance estimation, initiated by Saint-Blanquet [3] in 1970, has been extended to measurements by photothermal radiometry. For example, this method enabled to characterize crimped metal tubes [4].

In the present study, the different thermal resistances successively involved between liner and engine block have the following values: $4.2 \times 10^{-5}\,K\,m^2\,W^{-1}$ for the 2 mm-thick cast iron and $3.5 \times 10^{-5}\,K\,m^2\,W^{-1}$ for the 5 mm-thick aluminum.

Concerning the contact resistance, flash method with thermocouples measurements [5] gave a range from 2×10^{-5} to $3 \times 10^{-4}\,K\,m^2\,W^{-1}$, corresponding to equivalent air layers from 0.5 to 10 μm. These measurements fix the resolution required for a quantitative nondestructive technique to give some usable results. Both metals having a resistance of about $4 \times 10^{-5}\,K\,m^2\,W^{-1}$, the importance of a good contact at the interface is clear, in order to make the heat evacuation efficient to the cooling circuit.

The first step of the present work was to validate the nondestructive technique by a residual phase shift measurement. Then, the thermal resistance (or the equivalent air layer thickness) at cast iron–aluminum interfaces is identified by an inverse procedure using the Gauss–Newton parameter estimation method [6]. Finally, the method is applied to the characterization of a liner–engine block interface.

2. Description and validation of the experimental device

Fig. 1 illustrates the nondestructive experimental system developed by PSA. Under a controlled sinusoidal excitation from a set of four spotlights (ADB DW105, 1000 W each) electrically modulated, the thermal response is measured by means of an infrared camera. The illuminated area is about 30 cm diameter, and the flux is about $1000\,W\,m^{-2}$.

A numerical lock-in procedure, based on the post-treatment algorithm developed by Pron et al. [7,8] allows a significant improvement of the signal to noise ratio. It yields amplitude and absolute phase maps (thanks to the reference signal recorded via a photodiode) of the periodic thermal field, for modulation frequencies ranging from 10^{-3} Hz to a few Hz. This system allows the detection of very low temperature variations on the front surface of the element under test (for an acquisition of 300 images: 4.6 mK with an AGEMA 900 LW scanning camera

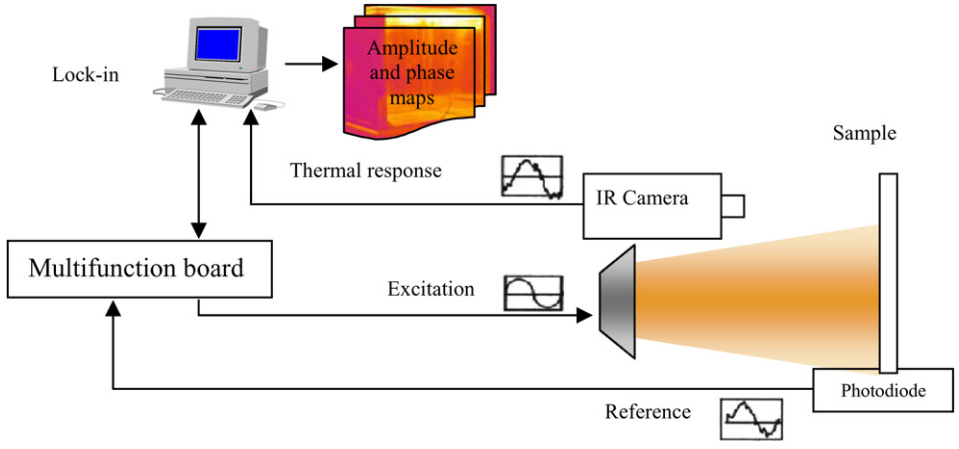

Fig. 1. Experimental set-up.

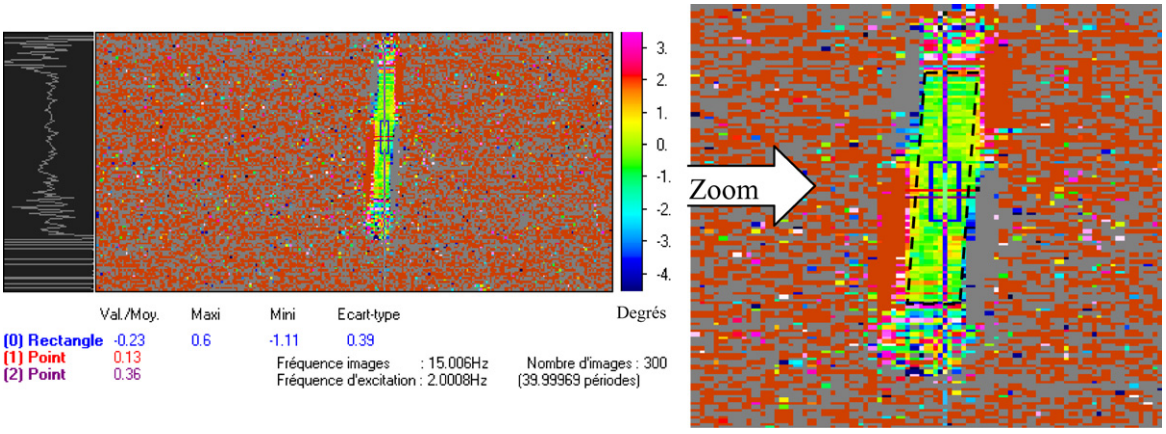

Fig. 2. Map of the residual phase shift.

and 1.1 mK with a THERMACAM SC3000 focal plane array camera).

A dedicated experimental configuration has been developed in order to validate the numerical lock-in procedure. This particular measurement, called "zero phase", concerns the residual phase shift between the response of the infrared camera and that of a HgCdTe point sensor, during the observation of the same periodic thermal phenomenon.

The sample used for this purpose is a 200 μm-thick metal strip. This strip is connected at the output of an electric generator, which provides a periodic excitation by Joule effect. Both the infrared camera and the HgCdTe sensor measure the strip thermal response. Obtaining phase values centered around zero confirms the good synchronization between photothermal and reference signals (provided respectively by IR camera and HgCdTe sensor), and guarantees the absolute phases availability.

The test bench associated with the AGEMA 900 LW camera was successfully tested for different measurement configurations (temperature ranges of the camera, modulation frequencies…). For a frequency of 2 Hz and on the 50–350 °C range, an average phase value of −0.23° with a standard deviation of 0.39° was obtained on the measurement area. The map of the residual phase shift is shown on Fig. 2.

When the test bench was used with the THERMACAM SC3000 camera, the measured average phase shift was −4.77° at 1 Hz. So, the "zero phase" condition was not verified with this camera. Moreover, it was not possible to get enough guarantee on the acquisition sequence (lack of images in some series, but also inaccuracy of the dating), and so to validate the lock-in procedure with this camera. This emphasizes the importance of a perfectly known camera acquisition timing for a lock-in procedure development. Consequently, the following results are all obtained with the AGEMA 900 LW scanning camera.

3. Thermal models and parameter estimation

A quantitative characterization using lock-in detection depends on the interpretation of absolute phase measurements, and then requires the development of appropriate thermal models.

3.1. Analytical models

The thermal phenomenon analysis was first realized by an analytical modeling of unidimensional semi-transparent multilayers. This model allows to calculate the sample response to a periodic excitation and to obtain the phase and amplitude theoretical values of the temperature response.

In order to increase and to homogenize the sample emissivity, an emissive deposit must be applied on the front surface, usually a sprayed paint. So, the sample is made up of an emissive layer (emissivity = 0.92) on a cast iron plate, which is separated from an aluminum plate by an air layer of variable thickness (Fig. 3). An equivalence was already established between a two-layer model with a contact thermal resistance and a three-layer model with a central air layer at the interface [9]. Similar results were obtained here with an additional layer representing the emissive deposit at the front surface. Thus, the resistances can be easily expressed in terms of equivalent air layer. The resistances being obtained by dividing the thickness by the thermal conductivity of air at rest (about 0.025 $\mathrm{W\,m^{-1}\,K^{-1}}$), the equivalent air layer thickness is $l\,(\mu\mathrm{m}) = 2.5 \times 10^4 \times R$.

The four-layer unidimensional model solves classically the heat diffusion equation with a sinusoidal heat source:

$$\Delta T_i(z,t) - \frac{1}{a_i}\frac{\partial T_i(z,t)}{\partial t} = -\frac{q_i(z,t)}{k_i} = -\frac{q_i(z)}{2k_i}\left(1 + e^{j\omega t}\right) \quad (1)$$

The solution for the temperature in each layer is searched under the form:

$$T_i(z,t) = T_{\mathrm{amb}} + T_{c,i}(z) + T_{a,i}(z).e^{j\omega t} \quad (2)$$

The radiative heat source $q_i(z)$ is obtained from the solution of the radiative transfer equation in each layer. The net radiative fluxes have the form:

$$\Phi_i(z) = \Phi_i^+(z) - \Phi_i^-(z) = P_i e^{-K_i z} - M_i e^{K_i z} \quad (3)$$

and the corresponding heat sources are:

$$q_i(z) = -\frac{\mathrm{d}\Phi_i(z)}{\mathrm{d}z} = K_i P_i e^{-K_i z} + K_i M_i e^{K_i z} \quad (4)$$

The constants M_i and P_i are obtained by matrix inversion from the radiative boundary conditions, corresponding to the reflections at the interfaces [10].

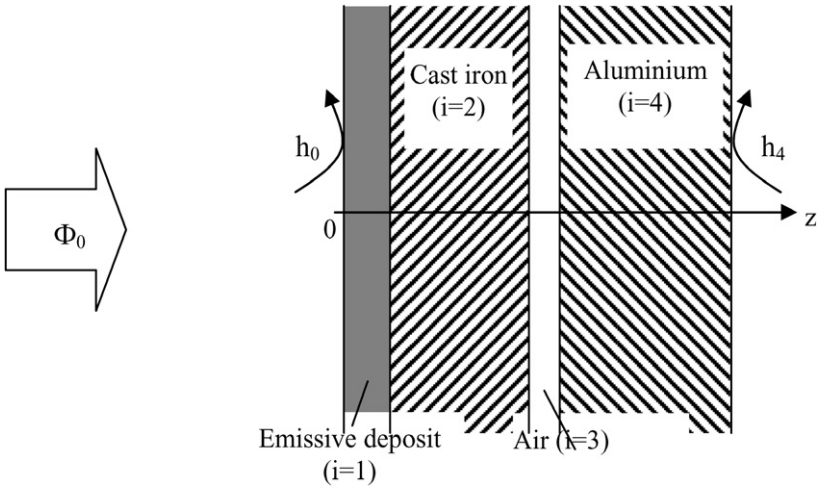

Fig. 3. Four-layer structure diagram.

The continuous component $T_{c,i}(z)$ of the temperature is solution of:

$$\frac{\mathrm{d}^2 T_{c,i}(z)}{\mathrm{d}z^2} = -\frac{q_i(z)}{2k_i} \tag{5}$$

and has the form:

$$T_{c,i}(z) = A_i z + B_i + C_i e^{-K_i z} + D_i e^{K_i z} \tag{6}$$

The constants are here obtained from the conductive or radiative–convective boundary conditions at the interfaces.

At $z = 0$,

$$-k_1 \left(\frac{\mathrm{d}T_{c,1}}{\mathrm{d}z}\right)_{z=0} = -h_0 T_{c,1}(0) \tag{7}$$

At $z = l_1$,

$$-k_1 \left(\frac{\mathrm{d}T_{c,1}}{\mathrm{d}z}\right)_{z=l_1} = -k_2 \left(\frac{\mathrm{d}T_{c,2}}{\mathrm{d}z}\right)_{z=l_1} \tag{8}$$

$$T_{c,1}(l_1) = T_{c,2}(l_1) \tag{9}$$

At $z = l_2$,

$$-k_2 \left(\frac{\mathrm{d}T_{c,2}}{\mathrm{d}z}\right)_{z=l_2} = -k_3 \left(\frac{\mathrm{d}T_{c,3}}{\mathrm{d}z}\right)_{z=l_2} \tag{10}$$

$$T_{c,2}(l_2) = T_{c,3}(l_2) \tag{11}$$

At $z = l_3$,

$$-k_3 \left(\frac{\mathrm{d}T_{c,3}}{\mathrm{d}z}\right)_{z=l_3} = -k_4 \left(\frac{\mathrm{d}T_{c,4}}{\mathrm{d}z}\right)_{z=l_3} \tag{12}$$

$$T_{c,3}(l_3) = T_{c,4}(l_3) \tag{13}$$

At $z = l_4$,

$$-k_4 \left(\frac{\mathrm{d}T_{c,4}}{\mathrm{d}z}\right)_{z=l_4} = h_4 T_{c,4}(l_4) \tag{14}$$

Once more, a matrix inversion gives the constants for each layer temperature.

The alternative component $T_{a,i}(z)$ is obtained in a similar way, starting from the heat equation:

$$\frac{\partial^2 T_{a,i}(z,t)}{\partial z^2} - \frac{1}{a_i}\frac{\partial T_{a,i}(z,t)}{\partial t} = -\frac{q_i(z,t)}{k_i} \tag{15a}$$

$$\frac{\mathrm{d}^2 T_{a,i}(z)}{\mathrm{d}z^2} e^{j\omega t} - \frac{j\omega}{a_i} T_{a,i}(z) e^{j\omega t} = -\frac{q_i(z)}{2k_i} e^{j\omega t} \tag{15b}$$

The solution has the form:

$$T_{a,i}(z) = E_i e^{-\sigma_i z} + F_i e^{\sigma_i z} + G_i e^{-K_i z} + H_i e^{K_i z} \tag{16}$$

with

$$\sigma_i = \sqrt{\frac{j\omega}{a_i}} = \frac{1+j}{\mu_i}$$

and should verify the same as above thermal boundary conditions. The constants are given again by matrix calculation [10].

A sensitivity study of the thermal response to the different parameters of the model allowed to more accurately determine the optimal experimental conditions for air layer detection at the cast iron–aluminum interface and to identify the key parameters for subsequent development of the inverse procedure. The first lesson learnt from this study is the important phase sensitivity of the photothermal response to thickness variations of the paint layer at the front face of the sample. So, another black and matt deposit, the phosphatation, the applying technique of which guarantees a controlled uniform thickness, efficiently replaces the black paint. Fig. 4 clearly shows the better uniformity of the phase maps obtained with a phosphatation layer.

The parameters used in the simulations are presented in Table 1 (at a mean temperature of 100 °C). Fig. 5 shows the evolution of the phase reduced sensitivity to the contact thermal resistance, versus modulation frequency. This reduced sensitivity is calculated as [6]:

$$\beta_i \frac{\partial \varphi(f,\beta)}{\partial \beta_i} = \beta_i X_i(f,\beta) \tag{17}$$

A detailed sensitivity study is available in [10]. The phase appears to be significantly sensible to the absorption coefficient of the emissive layer, but rather insensible to that of the metal. The values in Table 1 are rounded off from typical values of the extinction coefficients from the literature. Within the frequency range 0.01–2 Hz, the phase is insensible to the rear face

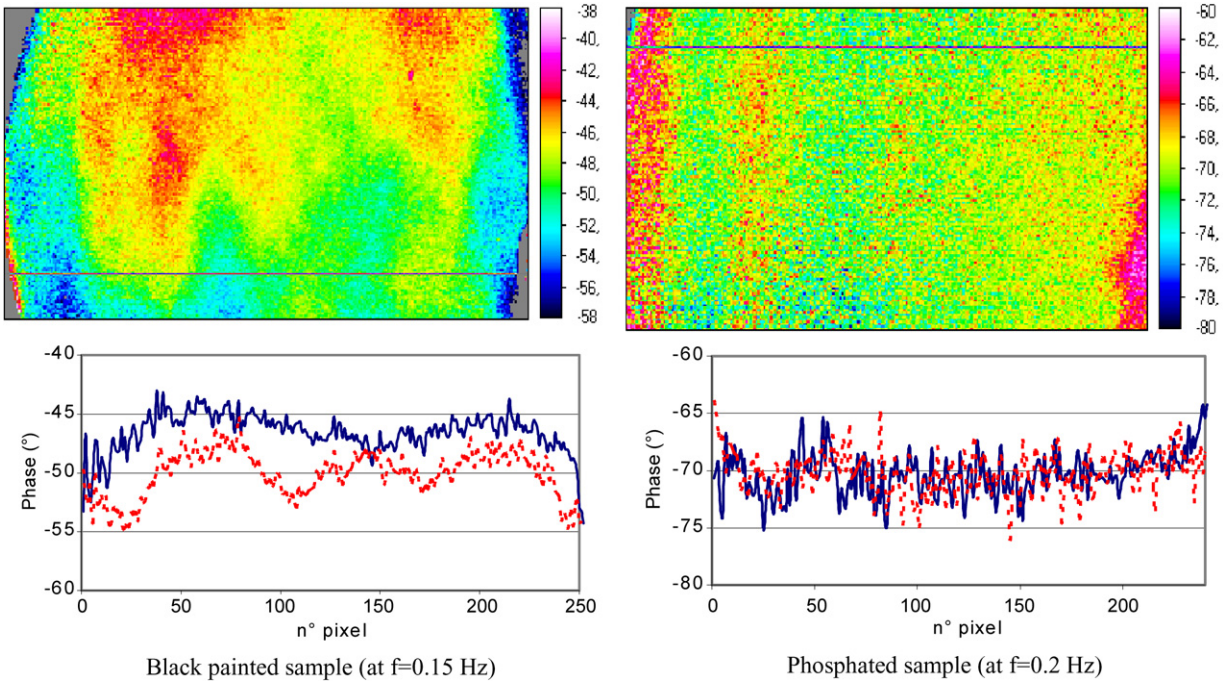

Fig. 4. Comparison between phase maps for the two surface preparations (painting and phosphatation).

Table 1
Parameters values used in the simulations

	Phosphatation	Cast iron	Air	Aluminum
Thickness (m)	17×10^{-6}	2×10^{-3}	5×10^{-6}	5×10^{-3}
Thermal conductivity ($W\,m^{-1}\,K^{-1}$)	1.781	47.3	0.0314	144
Density ($kg\,m^{-3}$)	1000	6987	0.954	2776
Specific heat ($J\,kg^{-1}\,K^{-1}$)	2000	525	1011	937
Optical absorption coefficient (m^{-1})	10^5	50×10^6		
Surface exchange coeff. ($W\,m^{-2}\,K^{-1}$)	25			10

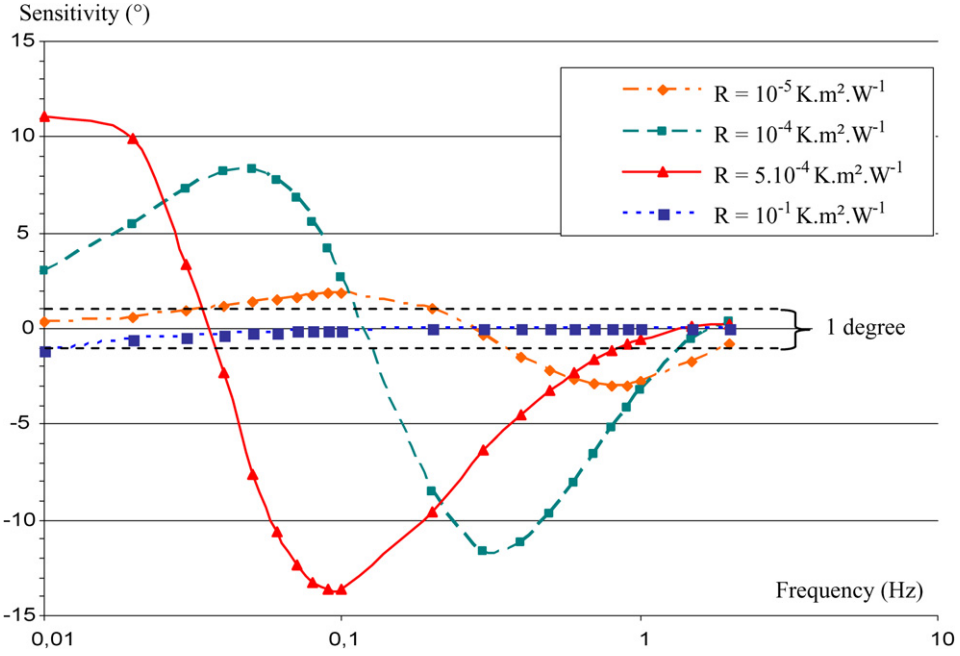

Fig. 5. Phase sensitivity evolution for different values of the thermal resistance.

exchange coefficient h_4 and sensible only at the lowest frequencies to the front face one h_0. The rear face value is evaluated as that of a classical radiative–convective exchange at room temperature, while the front face value arises from a dedicated study of the exchange coefficient in the presence of the sinusoidal irradiation [11].

The relevant frequency domain of investigation here ranges between 0.01 and 2 Hz. If the resistance increases beyond 4×10^{-3} K m^2 W^{-1} (100 μm-thick air layer), the phase sensitivity becomes nearly zero. The photothermal method proves to be particularly sensitive to resistance values between 4×10^{-6} and 4×10^{-3} K m^2 W^{-1} (equivalent air layer between 0.1 and 100 μm). In this range indeed, a resistance variation of 4×10^{-6} K m^2 W^{-1} corresponds to a phase shift of 1 degree, which is, as a first approximation, the accuracy of a phase measurement.

The use of a 1D analytical model supposes a uniform distribution of the incident flux across the whole sample surface. In practice, it is very difficult to scrupulously meet a 1D condition, especially for good heat conductors like metals. In order to consider the lateral diffusion effects introduced by a non-uniform incident flux, the modeling was then realized with an axis-symmetrical 2D analytical model. This kind of model [12] still describes the behavior of a sample structured in semi-transparent parallel layers, but irradiated by a Gaussian incident flux (Fig. 2.22).

The bi-dimensional heat diffusion equation in cylindrical coordinate system is [13]:

$$\frac{\partial^2 T_i(r,z,t)}{\partial r^2} + \frac{1}{r}\frac{\partial T_i(r,z,t)}{\partial r} + \frac{\partial^2 T_i(r,z,t)}{\partial z^2} - \frac{1}{a_i}\frac{\partial T_i(r,z,t)}{\partial t} = -\frac{q_i(r,z,t)}{k_i} \tag{18}$$

The incident flux is no more uniform, with a Gaussian radial shape:

$$\Phi_0(r,t) = I_0 e^{\left(-\frac{r^2}{r_0^2}\right)}\left(\frac{1+e^{j\omega t}}{2}\right) \tag{19}$$

The solution for the temperature is searched here under the form:

$$T_i(r,z,t) = T_{\text{amb}} + T_{c,i}(r,z) + T_{a,i}(r,z)e^{j\omega t} \tag{20}$$

The continuous and alternative components of the temperature are respectively solutions of:

$$\frac{\partial^2 T_{c,i}(r,z)}{\partial r^2} + \frac{1}{r}\frac{\partial T_{c,i}(r,z)}{\partial r} + \frac{\partial^2 T_{c,i}(r,z)}{\partial z^2} = -\frac{q_i(r,z)}{k_i} \tag{21}$$

$$\frac{\partial^2 T_{a,i}(r,z,t)}{\partial r^2} + \frac{1}{r}\frac{\partial T_{a,i}(r,z,t)}{\partial r} + \frac{\partial^2 T_{a,i}(r,z,t)}{\partial z^2} - \frac{j\omega}{a_i}T_{a,i}(r,z,t) = -\frac{q_i(r,z,t)}{k_i} \tag{22}$$

which are solved by separation of variables. The solutions of the associated homogenous equations are searched under the form $T(r,z) = F(r).G(z)$, then particular solutions of the complete equations are added.

The corresponding functions $F(r)$ and $G(z)$ are solutions of:

$$\begin{cases} F'' + \frac{1}{r}F' + m^2 F = 0 \\ G'' - \sigma_i^2 G = 0 \quad \text{with } \sigma_i^2 = m^2 + \frac{j\omega}{a_i} \end{cases} \tag{23}$$

For zero flux lateral boundary conditions, the amplitude is:

$$T_{a,i}(r,z) = \sum_{n=0}^{\infty} J_0(m_n r)\left(A_{i,n}e^{-\sigma_{i,n}z} + B_{i,n}e^{\sigma_{i,n}z}\right) \tag{24}$$

where the coefficients $A_{i,n}$ and $B_{i,n}$ are complex constants determined according to the thermal axial (z) boundary conditions at the four layer interfaces.

The radiative heat source in Eqs. (21) and (22) is developed on the basis of Bessel functions and the particular solution is:

$$T_{a,i}(r,z) = -\sum_{n=0}^{\infty} E_{i,n} J_0(m_n r)e^{-K_i(z+l_i)} \tag{25}$$

where the coefficients $E_{i,n}$ are obtained from matrix calculation, using the radiative boundary conditions at the interfaces.

Finally, the axis-symmetrical solution for the alternative temperature amplitude is completely determined as:

$$T_{a,i}(r,z) = \sum_{n=0}^{\infty} J_0(m_n r)\left[A_{i,n}e^{-\sigma_{i,n}z} + B_{i,n}e^{\sigma_{i,n}z} - E_{i,n}e^{-K_i(z+l_i)}\right] \tag{26}$$

3.2. Numerical model

Moving on to a multidimensional numerical model is essential to account for located defects at the cast iron–aluminum interface. An axis-symmetrical 2D numerical model, developed with ABAQUS™ finite element software, was firstly validated in a unidimensional configuration by comparison with the 1D analytical model [8].

Using a numerical model, it becomes possible to define a non-uniform thermal resistance. A localized resistive defect is thus simulated at the center of the sample. The two discs have a diameter of 100 mm; the cast iron plate is 3 mm-thick and the aluminium plate is 10 mm-thick. The lateral boundary conditions are convective–radiative with an exchange coefficient of 10 W m^{-1} K^{-1}.

The phase evolution along a radius, for a modulation frequency of 0.2 Hz and a uniform irradiation, is shown on Fig. 6. The phase values calculated outside the central transition area are close to the unidimensional ones. Due to the different resistance values on both sides of the gap, the transition area is not symmetrical.

The thermal diffusion length μ_i is defined as $(a_i/\pi f)^{1/2}$. It varies with the modulation frequency f and with the material thermal diffusivity a_i, and gives an order of magnitude for the penetration depth of the thermal oscillations. At a frequency of 0.2 Hz, this thermal diffusion length is 4.5 mm in cast iron. So, with a width of 15 mm, the transition area is about three times wider than the thermal diffusion length.

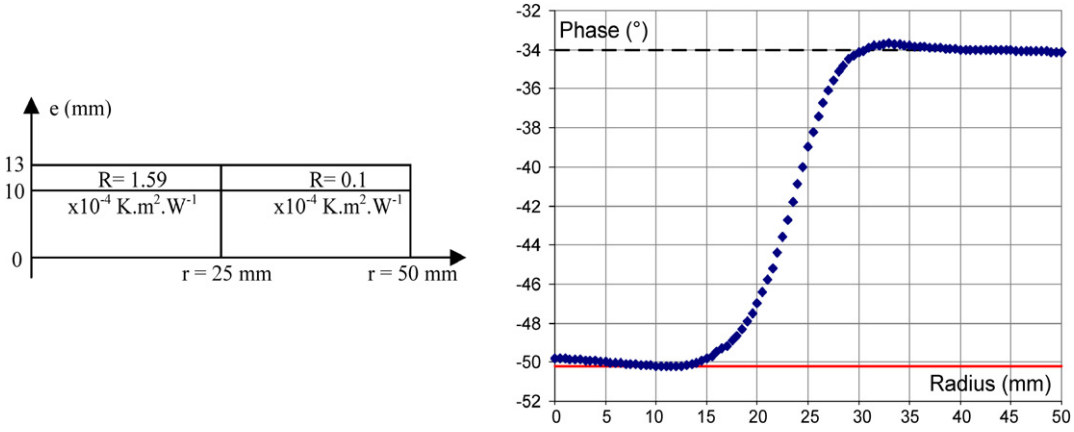

Fig. 6. Phase evolution along a sample radius.

3.3. Parameter estimation

The inverse procedure associated with these different models uses the Gauss–Newton parameter estimation method according to ordinary least squares [6]. The best adjustment with the experimental data provides a thermal resistance estimation as well as an associated confidence interval. These confidence intervals, resulting only from the theory–experiment adjustment, are given here with a risk of 10%.

Moreover, the inverse procedure associated with the numerical modeling requires a link between the finite element software and the parameter estimation program. The ABAQUS™ calculations are started and post-processed by the MATLAB™ software, which drives the minimization. This link was validated on simple profiles of thermal resistances, from simulated phase values [10].

4. Thermal resistance characterization

Since the functional installation of the nondestructive test bench has been completed, the study now focuses on academic samples representative of the liner–engine block interfaces.

The results have been obtained with series of 300 infrared frames quantized on 12 bit dynamics (ADDELIE system by ADDITIONAL Euro Technologies). Typically, the acquisition time of a sequence varies from 20 to 200 seconds, according to the modulation frequency, and 14 frequencies are used. The AGEMA 900LW scanner records the maps at a rate of 15 Hz. The thermal resistance is evaluated from the phase of the temperature response, less affected than the amplitude by the non-uniformity of the incident flux and by the local variations of optical absorption or emissivity [14].

4.1. First measurements of thermal resistances: simply joined plates

The first thermal resistance measurements were realized in a configuration where cast iron and aluminum plates are simply joined. Two cast iron plates of 250 mm diameter (useful area: 130 mm diameter) were used: the first one is 2 mm-thick and painted, the second one is 3 mm-thick and phosphated. Since these first tests only aimed to prove the ability of the method to measure contact resistances, only the 1D model was used here.

First series of measurements were realized with the coated cast iron plates alone. In this case, the coating thickness is measured thanks to a POSITECTOR 6000 (that allows a resolution of 1 μm), the cast iron properties are known, and the only remaining unknown in the two-layer analytical model is the thermal conductivity of the coating, identified by the inverse procedure. The volumic heats and exchange coefficients are set to the typical values of Table 1. Rigorously, the identified parameters should rather be the thermal diffusivity but conductivity has numerical values in $\mathrm{W\,m^{-1}\,K^{-1}}$ that are better adapted for the matrix inversion than those of the diffusivity in $\mathrm{m^2\,s^{-1}}$.

Second series of measurements have been realized with the cast iron plates joined to a 10 mm-thick aluminum plate: the plates are just brought to contact, without any applied stress. In this case, the inverse procedure provides the thermal resistance value at the metal–metal interface.

The results are grouped in Table 2. These first measurements of air layers between two joined plates gave air thicknesses of about 75 μm.

In the phosphated configuration, a simultaneous identification of the thermal resistance and of the cast iron thickness well retrieved the known thickness of the cast iron layer (2.97 ± 0.06 mm), with about the same resistance value of $(2.26 \pm 0.25) \times 10^{-3}\ \mathrm{K\,m^2\,W^{-1}}$ at the interface.

4.2. Dedicated mechanical device: straightened plates

In order to move towards the real motor interface, a specific mechanical device has been designed, allowing to apply a force on the sample perimeter while leaving an optical access at the centre of the front side. By this way, the plates (same characteristics as before) are straightened, apart from a slight convexity at the centre. Measurements of the relative gap between cast iron and aluminum plates are done by inductive displacement sensors: three sensors are at the plates perimeter, on the force transmission area, and one is at the centre of the free surface. The sensors are screwed in the aluminum plate and the total force applied to the sample is controlled. The source profile is

Table 2
Estimated coatings conductivities and thermal resistances

	Painted cast iron (2 mm)	Phosphated cast iron (3 mm)
Coating thermal conductivity ($W\,m^{-1}\,K^{-1}$)	0.360 ± 0.008	1.78 ± 0.24
Contact thermal resistance ($K\,m^2\,W^{-1}$)	$(1.97 \pm 0.07) \times 10^{-3}$	$(2.38 \pm 0.26) \times 10^{-3}$
Equivalent air layer thickness (μm)	62	75

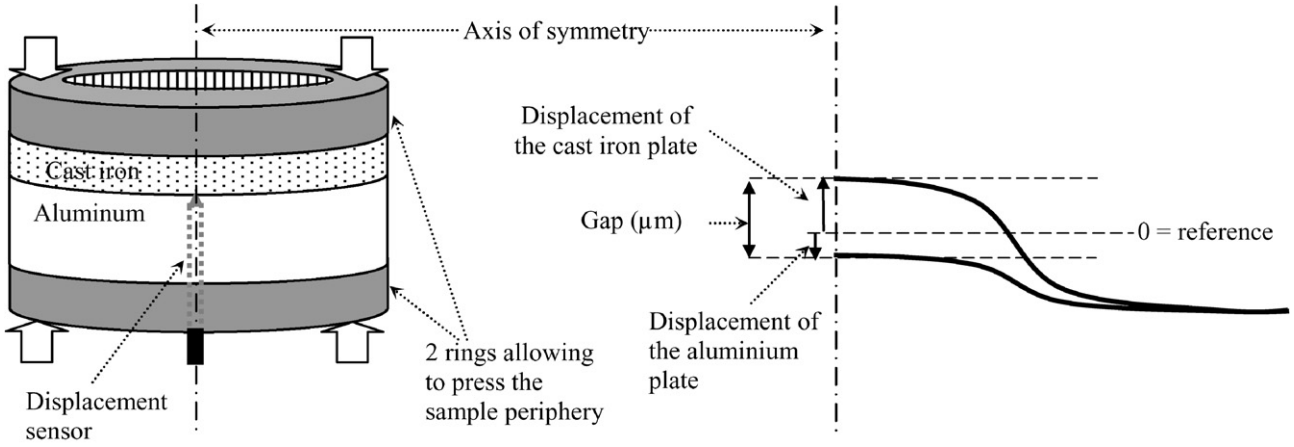

Fig. 7. Gap between cast iron and aluminum plates.

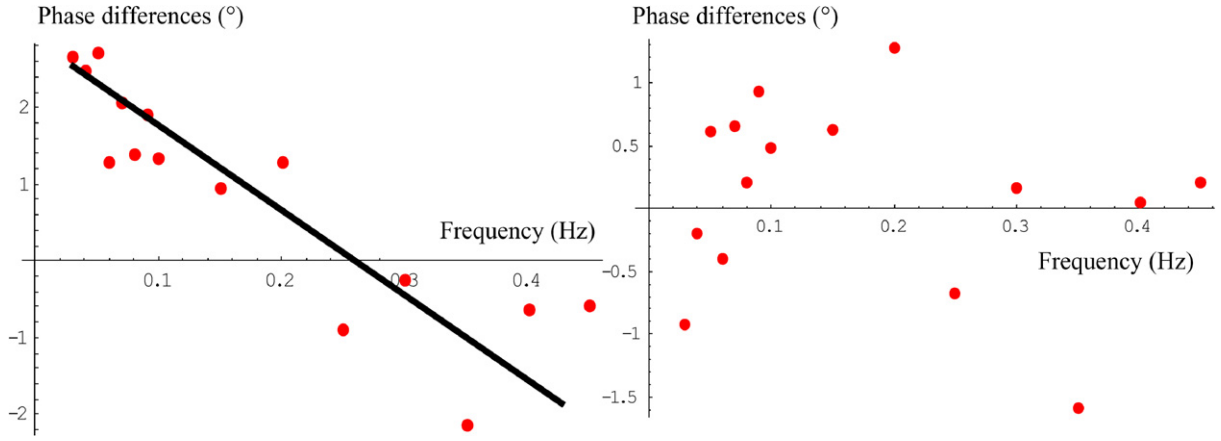

Fig. 8. Phase differences residuals—analytical 1D (left) and 2D (right) models.

deduced from the amplitude maps obtained on a phosphated cast-iron plate. Then, a 2D numerical model developed with ABAQUS™ software allows to calculate the mechanical behavior of the sample inserted in this test bench. With a load of 6 MPa on the sample perimeter and assuming the plates to be perfectly plane, smooth and unstressed in their initial conditions, the calculation provides a cast iron–aluminum gap of 2.86 μm at the centre (Fig. 7).

The average temperature level due to the use of the spotlights causes some additional deformations. A thermomechanical modeling with ABAQUS™ software gives a space of 4.57 μm at the interface centre, for a load of 6 MPa (250 kN) and a temperature rise at the front surface of 63 °C. So, the thermal contribution causes a gap increase of 60%. The temperature oscillations (a few °C) remain small enough to cause no significant variation of the gap (inferior to 0.1 μm).

4.3. Phosphatation characterization

The use of new plates in FT25 cast-iron requires once again to characterize the phosphatation by studying a phosphated cast iron plate alone. The coating thickness is measured (27 μm), the cast iron properties are known, and the only remaining unknown in the two-layer analytical model is the thermal conductivity of the coating.

In a first step, the estimation is realized with an 1D analytical model, but the correlation of the residuals (theory–experiment differences, Fig. 8) points out the inaccuracy of this model in this case. The implementation of the 2D model allows to take into account both the non-uniformity of the incident flux on this scale of work (the source profile being previously measured), and that of the thermal resistance. Then, a point to point identification gives a phosphatation thermal conductiv-

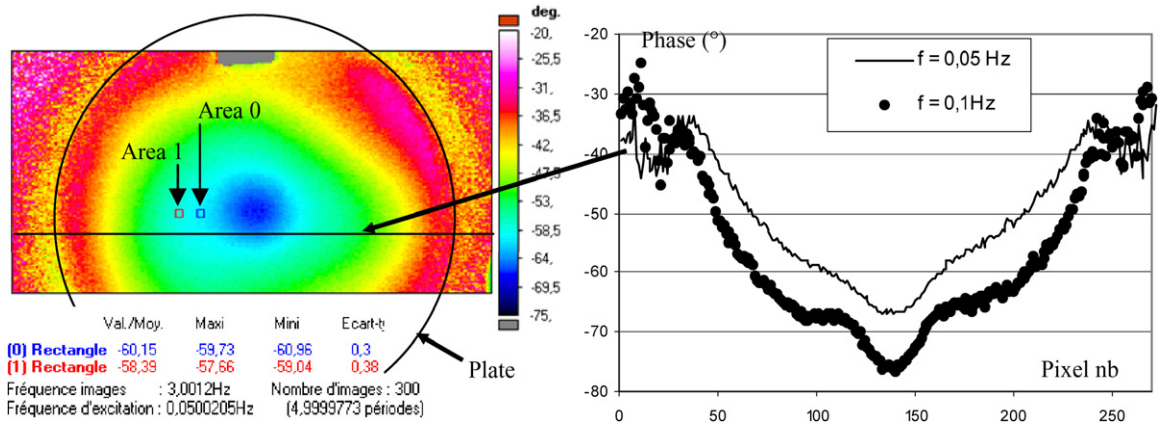

Fig. 9. Phase map at a modulation frequency of 0.05 Hz.

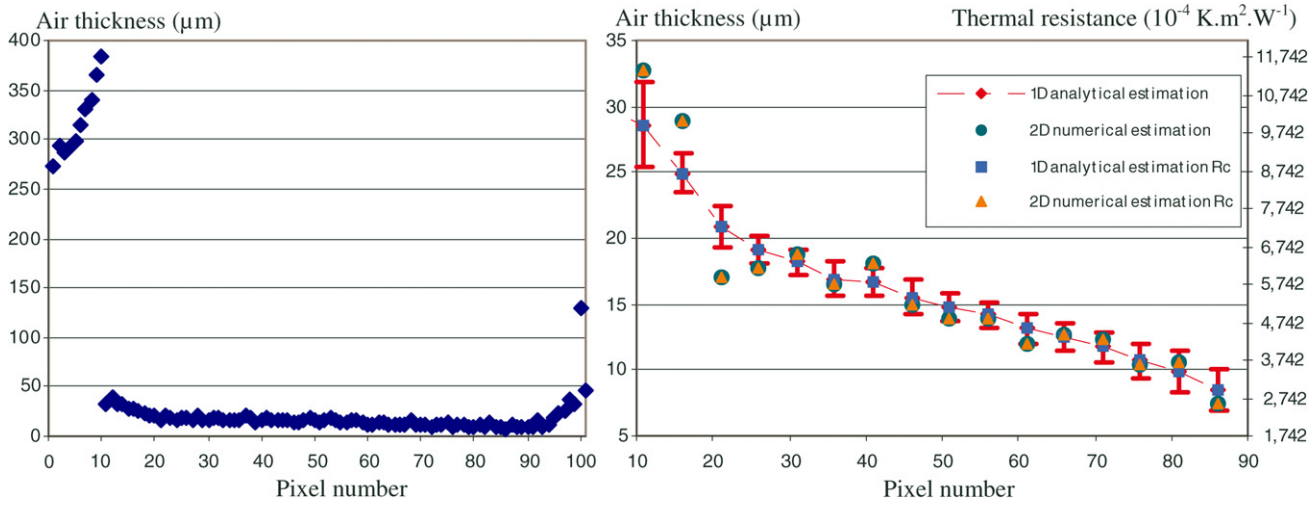

Fig. 10. Air thickness estimated along a horizontal radius (centre at pixel 0).

ity of 2.74 ± 0.28 W m^{-1} K^{-1} on a 2 mm-thick plate, and 2.88 ± 0.44 W m^{-1} K^{-1} on a 3 mm-thick plate. In the following, we keep a value of 2.8 W m^{-1} K^{-1} for the phosphatation thermal conductivity; one can note that the differences between these values and those obtained before are due to the fact that the substrate is different.

4.4. Thermal resistance profile identification

Fig. 9 represents the phase map for a modulation frequency of 0.05 Hz with a 2 mm-thick cast iron plate and a 10 mm-thick aluminum plate subjected to a force of 245.7 kN on their perimeter. In this case, both plates, actually not perfectly plane, are not simply joined but straightened out too. The central displacement sensor clearly appears on the figure, at the centre of the sample.

The air thicknesses estimated with a four-layer 1D analytical model on two measurement areas are 20.05 ± 0.73 µm and 19.04 ± 0.94 µm. These areas are chosen far enough from the centre to avoid being disturbed by the sensor presence.

The air layer thicknesses along a horizontal radius for a force of 245.7 kN are then estimated by both 2D numerical model and 1D analytical model. Fig. 10 shows that the clear breaking point due to the presence of the central displacement sensor is well retrieved. Beyond 18 mm from the centre (pixel 31), the comparison of the air layers estimated by both models points out that the 1D analytical model is sufficient to describe the sample behavior, thus justifying the choice of the two previous measurement areas.

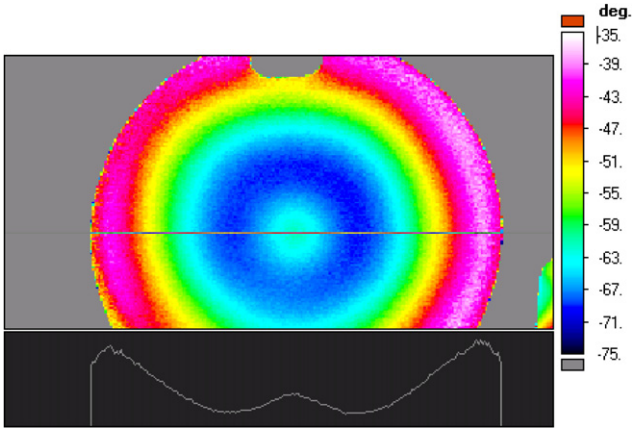

Fig. 11. Plates pressed at the centre: phase map at a frequency of 0.05 Hz.

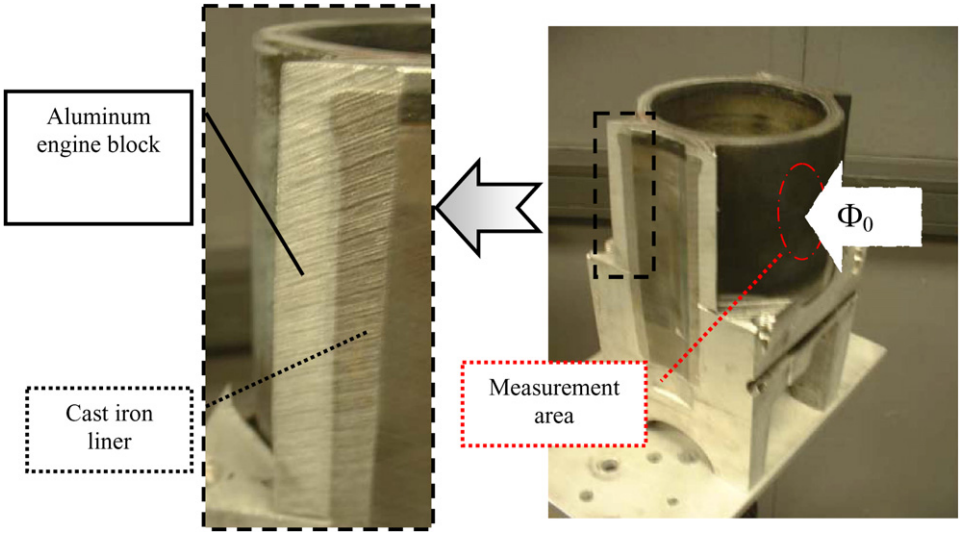

Fig. 12. Cut DV4 engine block.

With a force of about 150 kN applied on the sample perimeter, contact resistances ranging from 2.3×10^{-4} to 7×10^{-4} K m^2 W^{-1} are identified, equivalent to air layers ranging from 6.5 to 20 μm.

4.5. *Locally pressed plates*

In order to reach much lower thermal resistance values, it is necessary to apply a pressure at the interface. Bezerra Filho [15] measured resistances from 10^{-5} to 5×10^{-5} K m^2 W^{-1} at a copper–copper interface in vacuum and under loads of 5.79 and 2.21 MPa.

The use of a convex aluminum plate allowed us to force the cast iron plate (2 mm-thick) to come into close contact at the centre and no displacement sensor is needed. In this case, the pressed area is very localized (Fig. 11), thus the contact resistance is particularly non-uniform. The numerical inversion becomes more difficult as far as the thermal resistance profile is rather non-uniform and needs to be identified point by point (as in Section 4.2). Finally, the minimum thermal resistance estimated at the sample centre is about 1.65×10^{-5} K m^2 W^{-1}. This resistance value is in full agreement with the results given in the literature for samples under load [5,15–17].

5. Application to a liner–engine block interface

In order to test the measurement configuration of a real engine interface, contact thermal resistances were previously identified on an "inverted" academic sample that is made up of a painted 10 mm-thick aluminum front plate and a 3 mm-thick cast iron rear plate. In this case, the measured thermal resistances were found about 2 to 3×10^{-4} K m^2 W^{-1}, of the same order (however less accurate) than the ones previously got in the corresponding (but reverse) test conditions.

The method was finally applied to a DV4 cut engine block [8]. The cuttings were made as far as possible from the region to control (Fig. 12), in order to limit the disruptions at the interface. The phosphatation being difficult to realize on aluminum, the aluminum side (5.2 mm-thick) was black painted; the liner thickness was here 2.55 mm.

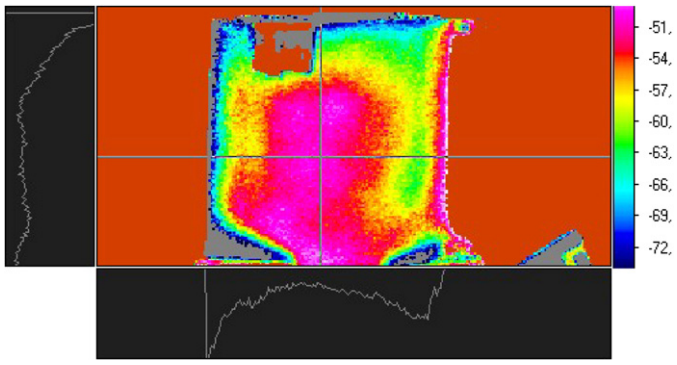

Fig. 13. Phase image obtained on a DV4 engine block (at a frequency of 0.06 Hz).

The photothermal measurements were realized at the point of maximal amplitude (Fig. 13); then, the inverse procedure, together with the 1D model, gave a thermal resistance of $2.67 \times 10^{-5} \pm 1.69 \times 10^{-5}$ K m^2 W^{-1}, that is equivalent to a 0.77 μm-thick equivalent air layer. A simultaneous estimation of the thermal resistance and of its depth provided an aluminum thickness of 5.03 ± 0.24 mm and a thermal resistance of $2.55 \times 10^{-5} \pm 0.9510^{-5}$ K m^2 W^{-1}. The thickness was identified here, since it brought some validation, the same identification procedure applied to the same experiment leading to the identification of the unknown thermal resistance, together with an exact value of the thickness.

The confidence intervals were rather large here, since the sensitivity of the method becomes low for these weak resistance values but also because of the experimental conditions (10 mm aluminum in front of 3 mm cast-iron).

As expected, the thermal resistance appears to be effectively weak in a real engine. Fortunately, the sensitivity of the method notably increases in the presence of a thicker air layer, the method being particularly relevant to defect detection.

6. Conclusion

After a validation of the nondestructive test bench by a residual phase shift measurement, the quantitative characterization of the contact thermal resistance at cast iron–aluminum interfaces has been realized successfully by means of the implementation of a numerical model linked to the parameter estimation software. The measured contact thermal resistances go down from 2×10^{-3} $\mathrm{K\,m^2\,W^{-1}}$ when the cast iron and aluminum plates are simply joined, to values between 2 and 7×10^{-4} $\mathrm{K\,m^2\,W^{-1}}$, when a force is applied on the plates perimeter, which are then straightened out.

Finally, when applied to a real liner–engine block interface, the method provides resistance values about 2×10^{-5} $\mathrm{K\,m^2\,W^{-1}}$, matching the values obtained when the cast iron plate is mechanically pressed against the aluminum plate. The different results obtained in this study are summarized on Fig. 14.

Such results are encouraging for potential industrial application of the method to the characterization of the liner–engine block interface, but a quantitative detection of 2D defects at the interface will require a 3D modeling to make the most of the phase maps.

The main drawback of the technique remains its time duration. Indeed, several hours are necessary for a precise identification of the thermal resistance, using more than ten modulation frequencies and waiting for thermal equilibrium between each one. For simple defect detection however, only one relevant frequency could be used then the duration reduced to a few minutes. An illustration is given on Fig. 15, where letters were cut in an aluminum foil then stuck at the interface under 2 mm-thick cast iron.

Such defects could probably be quantitatively investigated using the whole procedure, since the depth and value of the thermal resistance can be identified together. Moreover, using the whole thermographic map surely enables to determine the lateral extent of the defect.

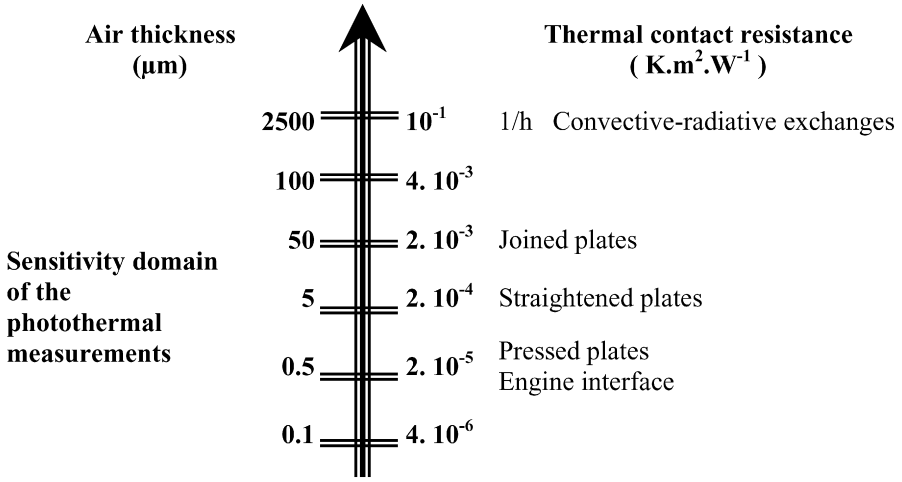

Fig. 14. Synthesis of the results.

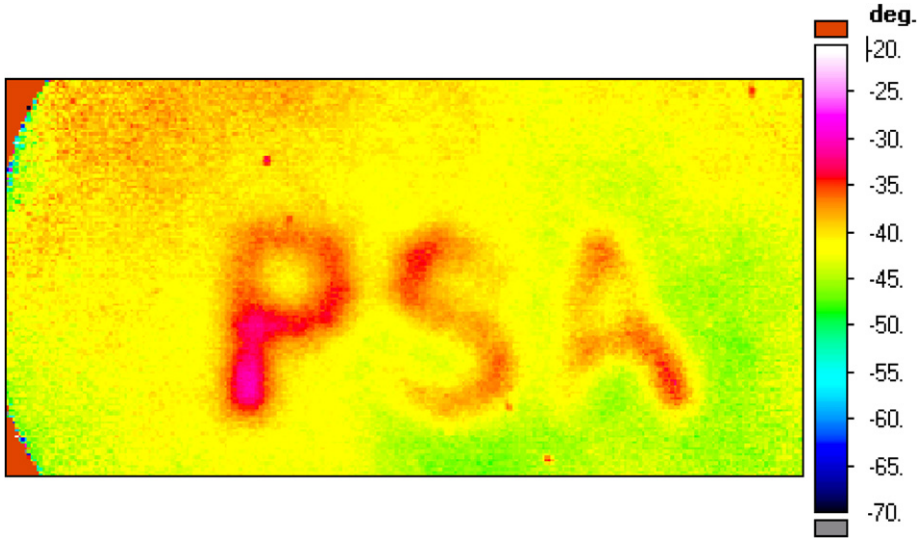

Fig. 15. Aluminum acronym « P S A » under 2 mm cast-iron: experimental phase map at 0.2 Hz.

References

[1] J.B. Saulnier, J. Taine, Quelques enjeux en transferts thermiques, Revue générale de thermique 37 (1998) 743–758.
[2] M. Laurent, Contribution à l'étude des échanges de chaleur au contact de deux matériaux, Thèse d'état, Lyon, 1969.
[3] C. Saint-Blanquet, Etude du transfert de chaleur entre deux solides accolés en régime thermique sinusoïdal, Thèse de doctorat, Nantes, 1970.
[4] E. Van Schel, M. Heuret, C. Bissieux, M. Regalia, M. Egee, A. Bailly, Résistance thermique de contact entre matériaux métalliques : mesure par radiométrie photothermique. Modélisation, expérimentation et application, Revue générale de thermique 36 (1992) 321–331.
[5] J.-C. Batsale, D. Stemmelen, A. Degiovanni, Utilisation de la méthode « flash » en géométrie cylindrique pour la mesure de résistance thermique d'un contact chemise bloc moteur, Journée SFT du 9 janvier 1991, Résistances de contact, Aspects industriels nouveaux, 1991.
[6] J.V. Beck, K.J. Arnold, Parameter Estimation in Engineering Science, Wiley, New York, 1977.
[7] H. Pron, J.F. Henry, S. Offermann, C. Bissieux, J.L. Beaudoin, Analysis of stress influence on thermal diffusivity by photothermal infrared thermography, QIRT 98 (Eurotherm No. 60), Lodz, 7–10 September 1998, pp. 129–133.
[8] H. Pron, C. Bissieux, 3D thermal modelling applied to stress-induced anisotropy of thermal conductivity, International Journal of Thermal Sciences 43 (12) (2004) 1161–1169.
[9] E. Van Schel, Radiométrie photothermique appliquée à la caractérisation et au contrôle de la résistance thermique de contact de métaux sertis, Thèse de Doctorat, Université de Reims, 1989.
[10] P. Laloue, Thermographie infrarouge photothermique appliquée à la caractérisation non destructive de l'interface chemise–bloc dans les moteurs automobiles, Thèse de Doctorat, Reims, 2003.
[11] P. Laloue, J. L'Ecolier, P. Dalarun, J.F. Henry, C. Bissieux, Application of modulated photothermal thermography to the determination of heat transfer coefficient profiles, in: Eurotherm Seminar 71: Visualization Imaging and Data Analysis in Convective Heat and Mass Transfer, Reims, 28–30 octobre 2002, pp. 229–234.
[12] H. Pron, Application des effets photothermiques et thermomécanique à l'analyse des contraintes appliquées et résiduelles. Utilisation d'une caméra infrarouge à mosaïque de détecteurs, Thèse de Doctorat, Université de Reims, 2000.
[13] M.N. Özisik, Heat Conduction, John Wiley & Sons, New York, 1993.
[14] D. Wu, G. Busse, Lock-in thermography for nondestructive evaluation of materials, Revue générale de thermique 37 (1998) 693–703.
[15] C.R. Bezerra Filho, Etude des résistances thermiques de contact en régime périodique, Thèse de doctorat, INSA Lyon, 1998.
[16] J.P. Bardon, Heat transfer at solid–solid interface, basic phenomenons, recent works, in: Fourth Eurotherm, vol. 1, Nancy, France, September 1988, pp. 40–74.
[17] L.S. Fletcher, Recent developments in contact conductance heat transfer, ASME Journal of Heat Transfer 110 (1988) 1059–1070.